Helix Unfolding in Unsolvated Peptides

Brian S. Kinnear, Matthew R. Hartings, and Martin F. Jarrold*

Contribution from the Department of Chemistry, Northwestern University, 2145 Sheridan Road, Evanston, Illinois 60208

Received December 7, 2000

Abstract: The conformations of unsolvated Ac-K$(AGG)_5$+H^+ and Ac-$(AGG)_5$K+H^+ peptides (Ac = acetyl, A = alanine, G = glycine, and K = lysine) have been examined by ion mobility measurements over a wide temperature range (150−410 K). The Ac-K$(AGG)_5$+H^+ peptide remains a globule (a compact, roughly spherical structure) over the entire temperature range, while both an α-helix and a globule are found for Ac-$(AGG)_5$K+H^+ at low temperature. As the temperature is raised the α-helix unfolds. Rate constants for loss of the helix (on a millisecond time scale) have been determined as a function of temperature and yield an Arrhenius activation energy and preexponential factor of 38.2 ± 1.0 kJ mol^{-1} and 6.5 ± 3.7 × 10^9 s^{-1}, respectively. The α-helix apparently does not unfold directly into the globule, but first converts into a long-lived intermediate which survives to a significantly higher temperature before converting. According to molecular dynamics simulations, there is a partially untwisted helical conformation that has both a low energy and a well-defined geometry. This special structure lies between the helix and globule and may be the long-lived intermediate.

Introduction

There have been many studies of helix formation by isolated peptides in aqueous solution. The vast majority of these measurements have probed equilibrium properties, such as the relative propensities of the different amino acids to form helices.[1−3] As alanine has a high helix-propensity in solution,[4−6] alanine-based peptides have been extensively studied. The mechanism of helix formation has received less attention. Helix formation is thought to occur through a process analogous to doing up a zipper: there is a slow initiation step (formation of the first helix turn) and a rapid propagation process (adding helical residues to the end of an existing helix).[7−9] Surprisingly, it is only in the last five years that the kinetics of helix folding and unfolding transitions have been examined for short peptides in aqueous solution. The first measurements were performed by Dyer and collaborators in 1996.[10] They examined the unfolding rate of Suc-AAAAA$(AAARA)_3$A-NH_2 (Suc = succinyl, A = alanine, and R = arginine) using laser-induced temperature jump and time-resolved infrared spectroscopy and found a relaxation time of 160 ns at 301 K. Thompson et al. have used laser-induced temperature jump with fluorescence monitoring to measure the unfolding rate of MABA-AAAAA-$(AAARA)_5$A-NH_2 (MABA = 4-(methylamino)benzoic acid).[8] The N-terminal fluorescent probe yielded a relaxation time of 20 ns. This fast relaxation time was attributed to unzipping the helix, while the slower relaxation time determined by Dyer et al. was attributed to the loss of entire helical segments.

More recently, Thompson et al. have used fluoresence quenching and laser-induced temperature jump to examine the unfolding of Ac-WAAAH-$(AAARA)_3$A-NH_2 (W = tryptophan and H = histidine).[9] The rate of helix unfolding increased with increasing temperature, with an apparent activation energy of around 33 kJ mol^{-1}. Asher and collaborators have used UV resonance Raman spectroscopy to probe the unfolding of AAAAA$(AAARA)_5$A by laser-induced temperature jump.[11] An activation energy of around 33 kJ mol^{-1} for unfolding was found in this work as well. Since the equilibrium constant for the helix ⇌ coil transition can be measured for these peptides, the folding rate can be deduced from the unfolding rate. The folding rates deduced in this way are around 10^6−10^8 s^{-1}.[8,10,11] Much slower folding rates were obtained from the stopped flow CD spectroscopy studies of Clarke and collaborators.[12] They found that Ac-YGAAKA$(AAAKA)_2$-NH_2 (Ac = acetyl, Y = tyrosine, G = glycine, and K = lysine) folds on a millisecond time scale. The origin of the difference between these results and the values deduced from the laser-induced temperature jump measurements is not known. Clarke et al. originally suggested that it was due to the stopped flow studies (which start with a chemically denatured peptide) measuring the much slower rate of helix initiation while the rate deduced from the laser-induced temperature jump studies is the rate of helix propagation.

Here we report the first experimental study of the kinetics of helix unfolding in an unsolvated peptide. There has been growing interest in examining the conformations and properties of unsolvated peptides and proteins because these vapor phase studies are expected to provide new insight into the role of

(1) Chakrabartty, A.; Baldwin, R. L. *Adv. Protein Chem.* **1995**, *46*, 141−176.
(2) Rohl, C. A.; Fiori, W.; Baldwin, R. L. *Proc. Natl. Acad. Sci. U.S.A.* **1999**, *96*, 3682−3687.
(3) Spek, E. J.; Olson, C. A.; Shi, Z. S.; Kallenbach, N. R. *J. Am. Chem. Soc.* **1999**, *121*, 5571−5572.
(4) Lyu, P. C.; Liff, M. I.; Marky, L. A.; Kallenbach, N. R. *Science* **1990**, *250*, 669−673.
(5) O'Neil, K. T.; DeGrado, W. F. *Science* **1990**, *250*, 646−651.
(6) Padmanabhan, S.; Marqusee, S.; Ridgeway, T.; Laue, T. M.; Baldwin. *Nature* **1990**, *344*, 268−270.
(7) Schwarz, G. *J. Mol. Biol.* **1965**, *11*, 64−77.
(8) Thompson, P. A.; Eaton, W. A.; Hofrichter, J. *Biochemistry* **1997**, *36*, 9200−9210.
(9) Thompson, P. A.; Muñoz, V.; Jas, G. S.; Henry, E. R.; Eaton, W. A.; Hofrichter, J. *J. Phys. Chem. B* **2000**, *104*, 378−389.
(10) Williams, S.; Causgrove, T. P.; Gilmanshin, R.; Fang, K. S.; Callender, R. H.; Woodruff, W. H.; Dyer, R. B. *Biochemistry* **1996**, *35*, 691−697.
(11) Lednev, I. K.; Karnoup, A. S.; Sparrow, M. C.; Asher, S. A. *J. Am. Chem. Soc.* **1999**, *121*, 8074−8086.
(12) Clarke, D. T.; Doig, A. J.; Stapley, B. J.; Jones, G. R. *Proc. Natl. Acad. Sci. U.S.A.* **1999**, *96*, 7232−7237.

10.1021/ja004196e CCC: $20.00
Published on Web 05/25/2001

intramolecular interactions and hydration interactions.[13−20] In recent work, we have shown how helix formation can be controlled in unsolvated peptides.[21,22] Ac-AnK+H^+ (n = 10−20) peptides, for example, form helices in the gas phase, while Ac-KA_n+H^+ (n = 10−20) do not. The lysine side chain carries the charge in these peptides, and when the lysine is at the C-terminus, the helix is stabilized by favorable interactions between the charge and the helix macrodipole[23,24] and by helix capping (where the protonated side-chain hydrogen-bonds to the dangling carbonyl groups at the C-terminus[25−27]). On the other hand, when the lysine is moved to the N-terminus, unfavorable charge−dipole interactions destabilize the helix, and the Ac-KA_n+H^+ peptides form globules (compact, roughly spherical structures).[28,29] Thus, moving the lysine between the N- and C-termini provides a convenient way of switching the helix on and off. In the Ac-K$(AGG)_5$+H^+ and Ac-$(AGG)_5$K+H^+ peptides studied here, the glycine residues are incorporated to destabilize the helical state. Glycine is known to be a helix-breaker in solution,[1] and the glycine analogues of the helical Ac-A_nK+H^+ peptides, Ac-G_nK+H^+, are globules in vacuo.[30] As we have shown elsewhere, a relatively large number of glycine residues are needed to destabilize the helical state of unsolvated alanine and glycine-based peptides.[31]

Experimental Methods

In the studies described here, information about the conformations of the unsolvated peptide ions is obtained from ion mobility measurements. Ion mobilities depend on the collision cross section between an ion and a buffer gas, which in turn depend on the geometry of the ion.[32−34] Structural information is obtained by comparing the cross sections derived from the mobilities to cross sections calculated for trial geometries obtained from MD simulations. The measurements were performed on a new, temperature-variable ion mobility apparatus shown schematically in Figure 1. The apparatus consists of an electrospray source, a temperature-variable drift tube, a quadrupole mass spectrometer, and a detector assembly. The electrospray emitter is a short length of 400 μm o.d. 250 μm i.d. deactivated fused silica capillary tubing. The emitter is held at around 3 kV with respect to a piece of stainless steel capillary tubing (10 cm long, 0.0508 cm i.d.). The steel capillary tube is mounted in a copper beryllium block that is heated to approximately 100 °C by cartridge heaters. The heated capillary tubing discharges into a small differentially pumped volume that is held at approximately 0.2 Torr by a mechanical booster pump. This region is connected to the main chamber through a small aperture. Ions that pass through the aperture are focused into the drift tube by an electrostatic lens.

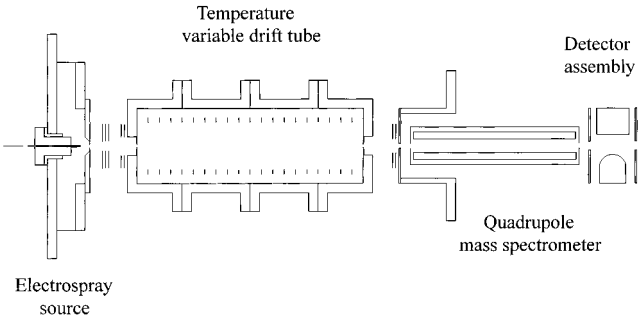

Figure 1. Schematic diagram of the temperature variable ion mobility apparatus.

The drift tube is designed to minimize temperature gradients. It consists of four copper beryllium sections, and the temperature of each section is regulated to better than 1 °C by microprocessor-based temperature controllers. It can be cooled to 77 K using liquid nitrogen and heated to 413 K using a closed loop recirculator containing a fluorocarbon. The drift tube is 25.4 cm long and contains a stack of field guard rings connected to a voltage divider to provide a uniform electric field along its length. The drift tube is usually operated with a drift voltage of 280−480 V and with a helium buffer gas pressure of around 4 Torr (at room temperature). These conditions are sufficient to ensure that the mobilities are measured in the low-field regime, where the mobility is independent of the field, and alignment effects are negligible. The ability to separate different conformations, the resolving power, is given approximately by[35]

$$\frac{t_{DT}}{t_{1/2}} = \frac{1}{4}\left(\frac{ze}{k_B \ln 2}\right)^{1/2}\left(\frac{V}{T}\right)^{1/2} \quad (1)$$

where t_{DT} is the drift time, $t_{1/2}$ is the width of the peak at half-height, ze is the charge on the ion, V is the drift voltage (the voltage drop across the drift tube), and T is the temperature. With the conditions employed here the resolving power at room temperature ($t_{DT}/t_{1/2}$) is around 36. This is considerably less than the resolving power available from our high-resolution ion mobility apparatus (∼180) that we have used to examine the conformations of unsolvated peptides at room temperature. However, it is more than sufficient to separate helices from globules.

After traveling across the drift tube some of the ions exit through a small aperture, they are then focused into a differentially pumped quadrupole mass spectrometer. After mass analysis the ions are detected by an off-axis collision dynode and dual microchannel plates. Drift time distributions are recorded by programming the quadrupole to transmit the relevant mass, and using an electrostatic shutter to modulate the ions from the source so that short (50 μs) packets of ions enter the drift tube. The arrival time distribution is recorded at the detector with a multichannel scaler employing a 10 μs dwell time. The drift time distribution is then obtained by correcting the arrival time distribution for the time that the ions spend traveling outside the drift tube, which is mainly the flight time from the drift tube exit to the detector. The drift times are converted into collision cross sections using[36]

(13) Suckau, D., Shi, Y.; Beu, S. C.; Senko, M. W.; Quinn, J. P.; Wampler, F. M.; McLafferty, F. W. *Proc. Natl. Acad. Sci. U.S.A.* **1993**, *90*, 790−793.
(14) Campbell, S.; Rodgers, M. T.; Marzluff, E. M.; Beauchamp, J. L. *J. Am. Chem. Soc.* **1995** *117*, 12840−12854.
(15) Schnier, P. D.; Price, W. D.; Jockusch, R. A.; Williams, E. R. *J. Am. Chem. Soc.* **1996**, *118*, 7178−7189.
(16) Kaltashov I. A.; Fenselau, C. *Proteins: Struct., Funct., Genet.* **1997**, *27*, 165−170.
(17) Valentine, S. J.; Clemmer, D. E. *J. Am. Chem. Soc.* **1997**, *119*, 3558−3566.
(18) Wyttenbach, T.; Bushnell, J. E.; Bowers, M. T. *J. Am. Chem. Soc.* **1998**, *120*, 5098−5103.
(19) Arteca, G. A.; Velázquez, I.; Reimann, C. T.; Tapia, O. *Phys. Rev. E* **1999**, *59*, 5981−5986.
(20) Schaaff, T. G.; Stephenson, J. L.; McLuckey, S. L. *J. Am. Chem. Soc.* **1999**, *121*, 8907−8919.
(21) Hudgins, R. R.; Ratner, M. A.; Jarrold, M. F. J. Am. Chem. Soc. **1998**, *120*, 12974−12975.
(22) Hudgins, R. R.; Jarrold, M. F. *J. Am. Chem. Soc.* **1999**, *121*, 3494−3501.
(23) Blagdon, D. E.; Goodman, M. *Biopolymers* **1975**, *14*, 241−245.
(24) Daggett, V. D.; Kollman, P. A.; Kuntz, I. D. *Chem. Scr.* **1989**, *29A*, 205−215.
(25) Presta, L. G.; Rose, G. D. *Science* **1988**, *240*, 1632−1641.
(26) Forood, B.; Feliciano, E. J.; Nambiar, K. P. *Proc. Natl. Acad. Sci. U.S.A.* **1993**, *90*, 838−842.
(27) Seale, J. W.; Srinivasan, R.; Rose, G. D. *Protein Sci.* **1994**, *3*, 1741−1745.
(28) Ihara, S.; Ooi, T.; Takahashi, S. *Biopolymers* **1982**, *21* 131−145.
(29) Shoemaker, K. R.; Kim, P. S.; York, E. J.; Stewart, J. M.; Baldwin, R. L. *Nature* **1987**, *326*, 563−567.
(30) Hudgins, R. R.; Jarrold, M. F. *J. Phys. Chem. B* **2000**, *104*, 2154−2158.
(31) Kaleta, D. T.; Jarrold, M. F. *J. Phys. Chem. B* Manuscript submitted.
(32) Hagen, D. F. *Anal. Chem.* **1979**, *51*, 870−874.
(33) von Helden, G.; Hsu, M.-T.; Kemper, P. R.; Bowers, M. T. *J. Chem. Phys.* **1991**, *95*, 3835−3837.
(34) Clemmer, D. E.; Jarrold, M. F. *J. Mass Spectrom.* **1997**, *32*, 577−592.
(35) Revercomb, H. E.; Mason, E. A. *Anal. Chem.* **1975**, *47*, 970−983.

$$\Omega_{avg}^{(1,1)} = \frac{(18\pi)^{1/2}}{16}\left[\frac{1}{m} + \frac{1}{m_b}\right]^{1/2} \frac{ze \quad t_D E_1}{(k_B T)^{1/2}\ L\ \rho} \qquad (2)$$

In this expression, m and m_b are the masses of the ion and buffer gas, ze is the charge on the ion, ρ is the buffer gas number density, L is the length of the drift tube, and E is the drift field.

$AcK(AGG)_5$ and $Ac(AGG)_5K$ were synthesized using *FastMoc* (a variant of Fmoc) chemistry on an Applied Biosystems model 433A peptide synthesizer. After cleaving with a 95% TFA (trifluoracetic acid)/5% water cocktail, the peptides were washed in water and lyophilized. The solutions for electrospraying were prepared by dissolving approximately 2 mg of peptide in 1 mL of TFA and 0.1 mL of water.

Results

Figure 2 shows a mass spectrum recorded for the $Ac(AGG)_5K$ peptide. The major peak at 1114 amu corresponds to $Ac(AGG)_5K+H^+$. The small peak at 1057 amu results from the deletion of a glycine residue. The peak due to the deletion of an alanine residue (at 1043 amu) is even smaller. In some spectra there was a fairly abundant peak corresponding to $Ac(AGG)_5K+Na^+$. Similar results were obtained for the $AcK(AGG)_5$ peptide.

Figure 3 shows drift time distributions recorded for $Ac(AGG)_5K+H^+$ as a function of temperature from 223 to 295 K. At 223 K and below, two well-separated peaks are present. Based on our previous studies of similar peptides, the peak at shorter drift time is assigned to a globule while the one at longer time is assigned to a helix. These assignments will be confirmed below. As the temperature is raised the peak at longer time gradually vanishes and at 282 and 295 K only a tail extending to longer times remains.

Figure 4 shows drift time distributions recorded from 295 to 409 K. As the temperature is raised, the tail evident in the 295 K distribution sharpens up to become a shoulder. The shoulder is clearly evident at 333 and 353 K and then starts to merge with the main peak as the temperature is raised further. For the $AcK(AGG)_5+H^+$ peptide only a single peak was observed over the entire temperature range examined (173 K to 408 K). This peak is assigned to a globule.

Figure 5 shows cross sections for the main features observed in the drift time distributions of $AcK(AGG)_5+H^+$ and $Ac(AGG)_5K+H^+$ plotted as a function of temperature. The cross sections for a given structure are expected to systematically decrease with increasing temperature because the long-range attractive interactions between the peptide ion and the buffer gas atoms become less important as the temperature is raised. The filled $AcK(AGG)_5+H^+$ points in Figure 5 show this type of temperature dependence. These points are due to a globule while the open $Ac(AGG)_5K+H^+$ points with cross sections above 270 Å^2 are due to a helix. At room temperature and below the cross sections for the $Ac(AGG)_5K+H^+$ peak with the shortest drift time overlap those measured for the $AcK(AGG)_5+H^+$ peptide. Above 310 K, however, the cross sections for these features diverge slightly. The middle set of cross sections in Figure 5 (including the open triangles) are discussed below.

Figure 6 shows the drift time distribution measured for globular $AcK(AGG)_5+H^+$ at 293 K. The dashed line shows the drift time distribution expected if the peptide had a single conformation. This was calculated from[36]

(36) Mason, E. A.; McDaniel, E. W. *Transport Properties of Ions in Gases*; Wiley: New York, 1988.

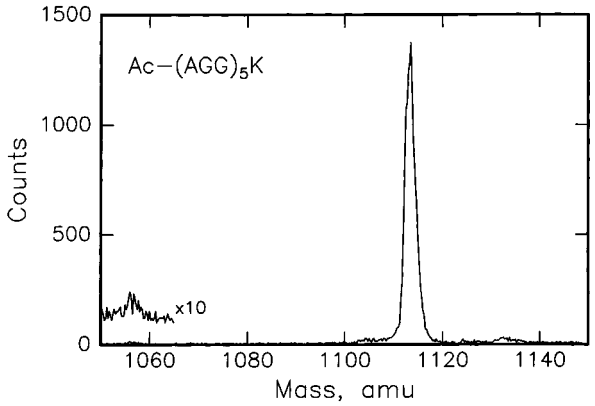

Figure 2. Mass spectrum recorded for the $Ac(AGG)_5K$ peptide.

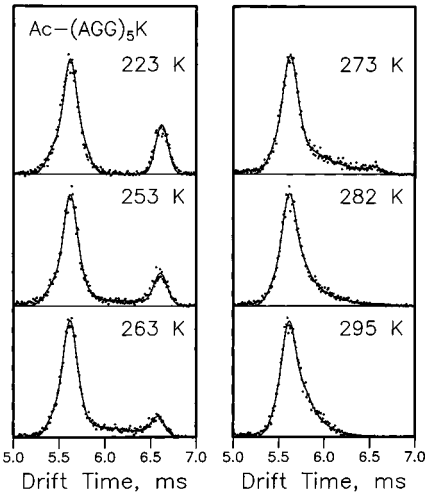

Figure 3. Drift time distributions recorded for $Ac(AGG)_5K+H^+$ as a function of temperature from 223 to 295 K. The points are the experimental data and the lines are the results of fits to the measured peaks (see Results).

$$\Phi(t) = \int dt_p P(t_p) \frac{C\,(v_D + L/t)}{(DT)^{1/2}}\left[1 - \exp\left(\frac{-r_o^2}{4Dt}\right)\right] \times \exp\left(\frac{-(L - v_D t)^2}{4Dt}\right) \qquad (3)$$

where C is a constant, v_D is the drift velocity, r_o is the radius of the entrance aperture, L is the length of the drift tube, $P(t_p)\,dt_p$ is the distribution function for the packet of ions entering the drift tube, and D is the diffusion constant. Under low-field conditions, D is given by Kk_BT/e where K is the mobility. Equation 3 accounts for the width of the ion packet injected into the drift tube and the spread of the ion packet by diffusion as it travels through the drift tube. The distribution calculated assuming a single conformation (the dashed line) clearly does not fit the measured peak very well. The solid line in the Figure, which provides a good fit to the measured peak, was obtained by averaging over the distribution of conformations represented by the histogram. The extent and intensity of the "tails" in the histogram were obtained from an automated fit to the experimental data using a least-squares criterion. These results indicate that there are a variety of slightly different globules which do not interconvert on the time scale of the experiment. As the temperature is raised, the measured peak becomes narrower, and as the temperature is lowered, it becomes broader. To fit the broader peaks obtained at lower temperatures, broader and more abundant "tails" are required. The globule peak for the

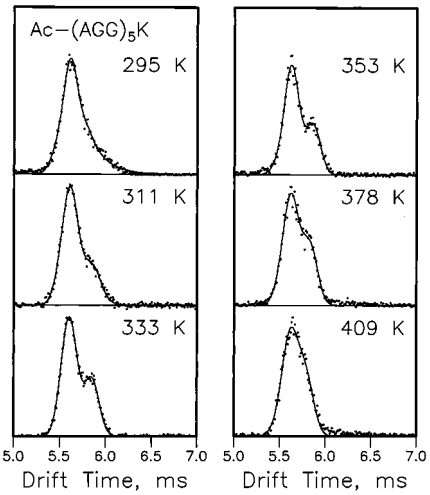

Figure 4. Drift time distributions recorded for $Ac(AGG)_5K+H^+$ as a function of temperature from 295 to 409 K. The points are the experimental data and the lines are the results of fits to the measured peaks (see Results).

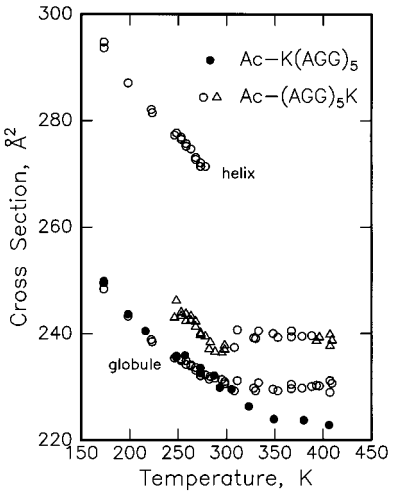

Figure 5. Cross sections for the main features in the drift time distributions for $AcK(AGG)_5+H^+$ (●) and $Ac(AGG)_5K+H^+$ (○ and △) as a function of temperature. The △ symbols represent values where the shoulder giving rise to the middle set of cross sections was not clearly apparent in the drift time distribution, and the cross section was derived from a fit to the data (see Discussion).

$Ac(AGG)_5K+H^+$ peptide can also not be represented by a single conformation; however, the peak assigned to the helix is narrower and can be adequately described by a single conformation even at low temperature (see Figure 3).

Determination of Rate Constants for Helix Unfolding

It is evident from the results shown in Figure 3 that as the temperature is raised the $Ac(AGG)_5K+H^+$ peak at long drift time (assigned to a helix) disappears and presumably converts into a peak at shorter drift time (assigned to a globule). Conversion of the helix into the globule must occur as the ions are traveling through the drift tube. Hudgins et al. have shown that under the appropriate conditions rate constants can be determined for conformational changes (isomerization processes) that occur as ions travel through a drift tube.[37] To illustrate how the rate constants are derived, Figure 7 shows drift time distributions calculated for a simple system consisting of two

(37) Hudgins, R. R.; Dugourd, Ph.; Tenenbaum, J. M.; Jarrold, M. F. *Phys. Rev. Lett.* **1997**, *78*, 4213−4216.

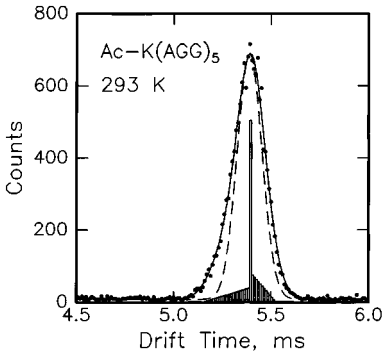

Figure 6. Drift time distribution for $AcK(AGG)_5+H^+$ at 293 K. The points are the measured distribution. The dashed line was calculated assuming a single conformation while the solid line was obtained assuming the distribution of conformations given by the histogram.

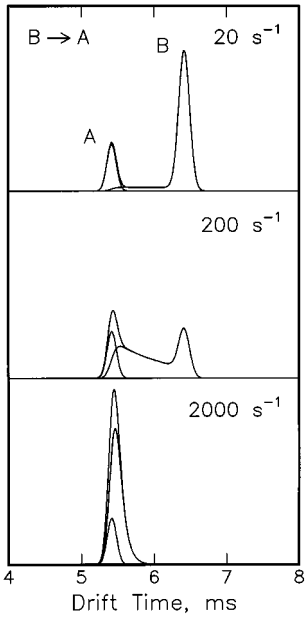

Figure 7. Drift time distributions calculated for different rates of conversion from B to A. Distributions are shown for peak A, peak B (including the B ions that convert to A as they travel across the drift tube), and the sum of these components.

components where the component at longer drift time (B) converts into the one at shorter drift time (A) as the ions travel through the drift tube. Drift time distributions calculated for the two components and their sum are shown for a range of different reaction rates. When conversion occurs slowly compared to the drift time, there are two well-separated peaks, as shown at the top of Figure 7 for a reaction rate of 20 s^{-1}. The low-intensity bridge between the two peaks results from ions that convert from B to A at different places along the length of the drift tube. The middle part of Figure 7 shows the situation when conversion occurs on a time scale comparable to the drift time. Peak B is significantly depleted as a large fraction of the B ions convert into A as they travel through the drift tube, and this is reflected in the large bridge between the two peaks. Ions in the bridge near peak A result from B ions that convert to A near the entrance of the drift tube (so that they spend most of their time as A ions). Ions in the bridge near peak B result from conversion near the drift tube exit (so that these ions spend most of their time as B). The lower part of Figure 7 shows the situation when the reaction occurs rapidly compared to the drift time. All of the B ions now convert to A ions close to the entrance of the drift tube, and there is no longer a separate B

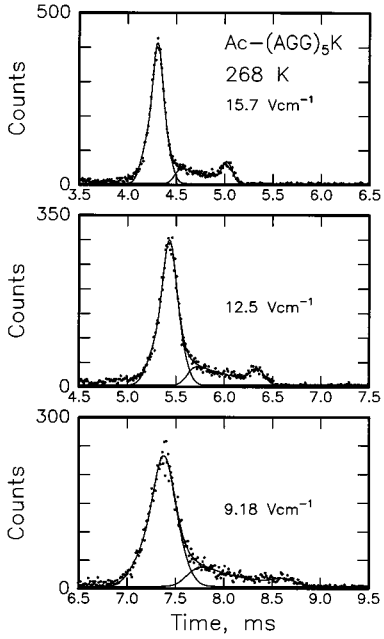

Figure 8. Drift time distributions recorded for $Ac(AGG)_5K+H^+$ at 268 K for a range of different drift voltages. The points are the experimental results. The lines are the results of simulations which account for the loss of the feature at long time. All three distributions were fit with a rate constant of 243 s^{-1}.

peak in the drift time distribution. The conversion from B ions to A ions is reflected in the exponential tail that extends to longer time. At higher rates of conversion the tail ultimately disappears, leaving only a single narrow peak.

By fitting the measured drift time distributions it is possible to determine rate constants for the conformational changes. An example is shown in Figure 8 which shows drift time distributions measured for $Ac(AGG)_5K+H^+$ at 268 K for a range of different drift voltages. Changing the drift voltage changes the amount of time that the ions spend in the drift tube and hence changes the amount of time available for conversion between the different conformations. The solid lines in the figure are fits to the measured distributions using the same rate constant for conversion (243 s^{-1}). The fits were done automatically using a least-squares criterion. The positions and intensities of the peaks were adjusted, along with the intensity and extent of the "tails" on the globule peak. The broadening of each component in the drift time distribution due to diffusion and the finite width of the injected pulse of ions were taken into account using eq 3.

Initial attempts to fit the drift time distributions, assuming the peak at longer time (the helix) converted directly into the peak at shorter time, did not yield sensible results. To understand what is happening it is necessary to examine the results shown in Figures 3 and 4 more closely. As the temperature is raised, the peak assigned to the helix disappears. At 282 K the helix peak is gone, leaving behind an exponential tail extending to longer time. As the temperature is raised further (see Figure 4), the helix starts to unfold as soon as it enters the drift tube, and the tail sharpens-up to reveal a shoulder at a slightly longer time than the main peak. It seems that the helix first converts into this feature, a long-lived intermediate which survives to significantly higher temperature, before eventually converting into the $Ac-(AGG)_5K+H^+$ globule (see below). The fits shown in Figure 8 were made assuming that the helix initially converts into a long-lived intermediate with approximately the same drift time as that of the shoulder (the drift time of the intermediate

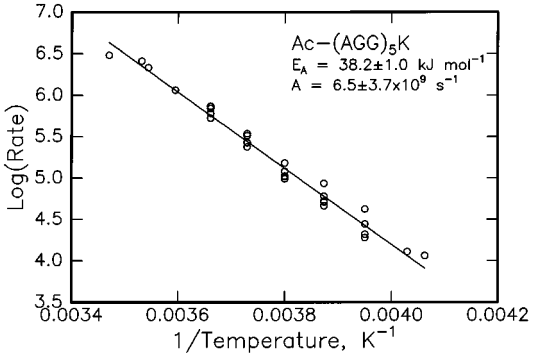

Figure 9. Arrhenius plot of log k against $1/T$ for loss of the $Ac(AGG)_5K+H^+$ helix.

was an adjustable parameter in the least-squares fit). With this assumption, sensible fits could be obtained over a wide temperature range and with different drift voltages, as illustrated in Figures 3 and 8. Note that the bridges between the peaks in Figure 8 stop short of the peak maximum because the product (the long-lived intermediate) is at a slightly longer drift time than the large peak.

We were able to obtain reliable rate constants for the loss of the helix from 248 to 288 K. Outside this temperature range the rates were either too fast or too slow to obtain a meaningful fit to the data. The temperature dependence of rate constants can usually be described using the empirical Arrhenius relationship,

$$k = A \exp(-E_A/k_B T) \qquad (4)$$

where A is the preexponential factor and E_A is the activation energy. An Arrhenius plot of log k against $1/T$ is shown in Figure 9. The results fall on a good straight line ($r^2 = 0.98$). A least-squares analysis yields an activation energy of 38.2 ± 1.0 kJ mol^{-1} and a preexponential factor of 6.5 ± 3.7 × 10^9 s^{-1}.

The analysis of the drift time distributions described above is based on the assumption that we are dealing with a two-state system; in this case, the helix and the long-lived intermediate. A test for the validity of this assumption is to adjust the drift voltage to change the time the ions spend in the drift tube. The rate constant derived from the drift time distributions should be independent of the reaction time. It is evident from the results shown in Figure 8 that a single value for the rate constant provides a good fit to drift time distributions measured with a range of drift voltages. However, slightly different values for the rate constants result if the drift time distributions are fit individually. The change in the quality of the fits when the drift time distributions are individually fit is usually so small that it is often difficult to discern a difference by eye. On the other hand, the differences in the rate constants appear to be systematic. Hence the assumption of a two-state system appears to be a good approximation, but it is not completely valid. Deviations from ideal behavior can result from three main causes. First, the presence of different populations of helices (with similar cross sections) that melt at slightly different rates. Second, the presence of one or more intermediates between the helix and shoulder with a lifetime that is less than (but not much less than) the drift time. And third, a back reaction which will eventually lead to an equilibrium between the different conformations. There is no real indication which of these factors is responsible for the small deviations from ideal behavior found here.

At 295 K and above the helix unfolds so rapidly that a reliable value for the unfolding rate cannot be derived from the data.

The fits to the experimental data shown in Figure 4 for temperatures of 295−353 K were obtained using rate constants extrapolated from the Arrhenius analysis. The tail evolves into the shoulder over this temperature range. The extrapolated rates account for the evolution of the shoulder quite well. At temperatures above around 370 K the shoulder begins to disappear as it converts into the globule. We attempted to determine rate constants for the loss of the shoulder; however, these attempts were not very successful because the peaks are too close together. It is possible that the shoulder and the main peak merge (in other words, the two structures interconvert) instead of the shoulder just converting into the main peak. We attempted to fit the high-temperature data for the Ac-$(AGG)_5K+H^+$ peptide, assuming that the peaks merge, but we could not obtain a unique fit. Different data sets gave widely different values for the forward and backward reaction rates.

Molecular Dynamics Simulations

A series of molecular dynamics (MD) simulations were performed to help identify the features observed in the drift time distributions. The MD simulations were performed using the MACSIMUS suite of programs[38] with the CHARMM force field (21.3 parameter set).[39] The bond lengths were constrained by SHAKE,[40] and the CH, CH_2, and CH_3 groups were treated as united atoms.[41] A time step of 1 fs was used, along with a dielectric constant of 1.0. The temperature was maintained by re-scaling the kinetic energies every 0.1 ps. Two sets of simulated annealing runs were performed, one terminating at 300 K and the other terminating at 400 K. The annealing schedules employed were 240 ps at 600, 500, and 400 K followed by 480 ps at 300 K and 240 ps at 600 and 500 K, followed by 480 ps at 400 K. In previous work, these relatively gentle annealing schedules seemed to do best at the difficult task of locating compact low-energy globule conformations.[42] An α-helix and a fully extended all-trans geometry were used as starting conformations for the simulated annealing runs. The simulations started from the near-linear all-trans geometry usually collapsed to globules, although some partially helical conformations also resulted. In addition, a series of 960 ps simulations were performed for the Ac-$(AGG)_5K+H^+$ peptide at 300 and 400 K starting from both an α-helix and a π-helix. A π-helix has i , $i + 5$ hydrogen bonds (4.4 residues per turn) compared with i , $i + 4$ hydrogen bonds (3.6 residues per turn) for an π-helix. The simulations started from an ideal π-helix quickly relaxed to an α-helix or a partial π-helix. Average cross sections for comparison with the measured values were obtained by calculating cross sections for 50 snapshots equally spaced over the last 35 ps of each MD simulation. The cross sections were calculated using the modified exact hard spheres scattering model.[42] If the conformations derived from the MD simulations are correct, the measured and calculated cross sections are expected to agree to within 2%. Average energies were also derived from the last 35 ps of each simulation.

Figure 10 shows the average energies plotted against the calculated cross sections for the 300 K simulations and the simulated annealing runs that terminated at 300 K. The open points show the results for the AcK$(AGG)_5+H^+$ peptides. The simulations for these peptides all collapsed to globules. As expected, a protonated lysine at the N-terminus destabilizes the helical conformation. The calculated cross sections for the globules are around 230−245 Å^2, with the low-energy ones having cross sections around 233 Å^2. This is close to the measured value of 230 Å^2 (see Figure 4). A more extensive set of simulations may yield slightly more compact and lower energy Ac$(AGG)_5+H^+$ conformations that are in even better agreement with the measured values.

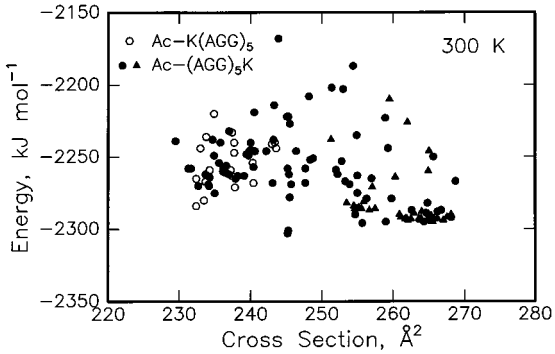

Figure 10. Plot of the average energy against cross section for the simulations performed for Ac-K$(AGG)_5+H^+$ and Ac$(AGG)_5K+H^+$ at 300 K. For Ac$(AGG)_5K+H^+$ results are shown for simulated annealing runs terminating at 300 K (●) and for MD simulations at a fixed temperature (▲). For Ac-K$(AGG)_5+H^+$ the results are from simulated annealing runs terminating at 300 K (○).

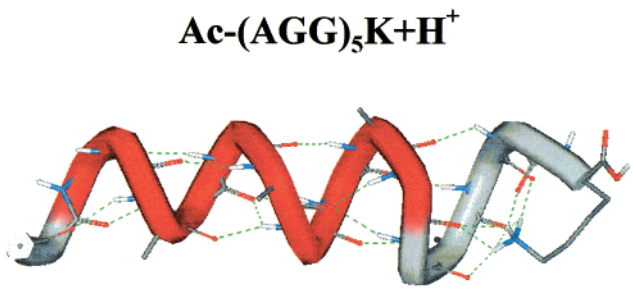

Figure 11. An example of an α-helical conformation from the MD simulations performed at 300 K. The conformation shown in the figure had an average energy of −2294 kJ mol^{-1} and an average cross section of 267 Å^2. The red regions are α-helix according to the WebLab viewer (Molecular Simulations Inc., San Diego, CA) used to produce the image.

The filled points in Figure 10 are the results of simulations for the Ac$(AGG)_5K+H^+$ peptide. The filled circles are from the simulated annealing runs, while the triangles are from the MD simulations performed at a fixed temperature. Some of the simulated annealing runs (mainly those from linear starts) have collapsed into globules with cross sections and energies similar to those found for the AcK$(AGG)_5+H^+$ globules. However, the Ac$(AGG)_5K+H^+$ peptides clearly occupy a much wider range of conformations. The clump of low-energy points with cross sections between 260 and 270 Å^2 are predominantly α-helical. An example of one of these conformations is shown in Figure 11. While the helices do not persist up to 300 K in the experiments, a short extrapolation indicates that they should have cross sections of around 266 Å^2 at 300 K, which is in close agreement with the calculated values for the α-helices. The low-energy conformations with cross sections around 255 Å^2 consist of a variety of helical structures, including some partial π-helices (usually with π-helix toward the C-terminus and α-helix toward the N-terminus since this provides an extra dangling carbonyl group for hydrogen bonding to the protonated lysine side chain). These helical structures have cross sections which deviate

(38) Kolafa, J. http://www.icpf.cas.cz/jiri/macsimus/default.htm.
(39) Brooks, B. R.; Bruccoleri, R. E.; Olafson, B. D.; States, D. J.; Swaminathan, S.; Karplus, M. *J. Comput. Chem.* **1983**, *4*, 187−217.
(40) Van Gunsteren, W. F.; Berendsen, H. J. *Mol. Phys.* **1977**, *34*, 1311−1327.
(41) Weiner, S. J.; Kollman, P. A.; Case, D. A.; Singh, U. C.; Ghio, C.; Alagona, G.; Profeta, S.; Weiner. P. *J. Am. Chem. Soc.* **1984**, *106*, 765−784.
(42) Kinnear, B. S.; Kaleta, D. T.; Kohtani, M.; Hudgins, R. R.; Jarrold, M. F. *J. Am. Chem. Soc.* **2000**, *122*, 9243−9256.

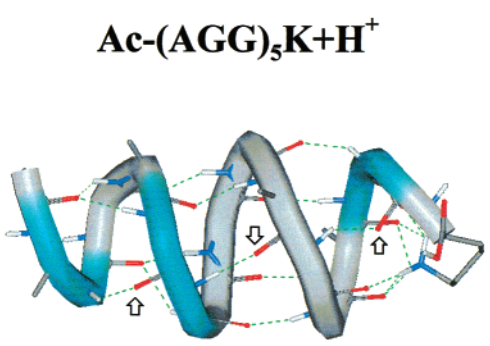

Figure 12. The most stable conformation found in the MD simulations performed at 300 K. Note the row of hydrogen bonds between backbone CO groups (sticks with red tips) pointing toward the N-terminus and backbone NH groups (sticks with white tips) pointing toward the C-terminus. The backward pointing CO groups are indicated by arrows. The blue regions are β-sheet according to the WebLab viewer (Molecular Simulations Inc., San Diego, CA) used to produce the image.

significantly from the extrapolated cross section from the experiments (266 Å^2).

The lowest-energy conformation in Figure 10 has a cross sections of around 245 Å^2. There is another point close by with almost the same cross section and energy, and its conformation is almost identical to the lowest-energy one (which is shown in Figure 12). The lowest-energy conformation found in the simulations performed at 400 K is almost identical to that shown in Figure 12. In the 400 K simulations, three runs led to this structure. The conformation in Figure 12 is a partially untwisted helix with predominantly i, $i + 6$ hydrogen bonding. A close inspection of Figure 12, however, reveals that some of the backbone CO groups point toward the N-terminus (the backward pointing ones are indicted by arrows) and some of the backbone N−H groups point toward the C-terminus. This leads to a row of hydrogen bonds pointing in the wrong direction for a normal helix, and gives the hydrogen-bonding network some β-sheet character (as indicated by the blue regions in the figure). The residues involved in this row of backward hydrogen bonds are exactly the same in all five low-energy structures found at both 300 and 400 K. This is clearly a special structure, in the sense that it has both a low energy and a well-defined geometry.

Discussion

Only a single feature was observed in the drift time distributions for the Ac-K(AGG)$_5$+H$^+$ peptide. The average cross sections decrease smoothly with increasing temperature (as long-range interactions between the ion and buffer gas become less important) and at 300 K they are close to values obtained from MD simulations of globular conformations. Three different features are observed for the Ac-(AGG)$_5$K+H$^+$ peptide. Below 300 K, one set of cross sections for Ac-(AGG)$_5$K+H$^+$ is coincident with the Ac-K(AGG)$_5$+H$^+$ globules, so these must be due to Ac-(AGG)$_5$K+H$^+$ globules. The cross sections for the Ac-K(AGG)$_5$+H$^+$ and Ac-(AGG)$_5$K+H$^+$ globules start to diverge slightly above 300 K. While obviously indicating slightly different structures, the nature of the difference is not clear at present. Cross sections determined from the 300 and 400 K simulations do not show a significant difference between the Ac-K(AGG)$_5$+H$^+$ and Ac-(AGG)$_5$K+H$^+$ globules. Thus, the simulations provide no insight into the origin of the difference.

The middle set of cross sections for the Ac-(AGG)$_5$K+H$^+$ peptide in Figure 5 is due to the shoulder. The shoulder is only clearly visible over a relatively narrow temperature range (around 310−390 K). However, outside of this range its position can be deduced from fits to the measured drift time distributions. The values deduced from the fits, when no clear shoulder was evident in the drift time distributions, are shown by open triangles in Figure 5. The open triangles between around 250−300 K represents the product from loss of the helix (the long-lived intermediate). These points appear to extrapolate to the shoulder observed at slightly higher temperature. However, the temperature dependence of this feature is not straightforward (the cross sections do not systematically decrease like those for the Ac-K(AGG)$_5$+H$^+$ globule) which may indicate that the intermediate at lower temperatures and the shoulder at higher temperatures do not have the same conformation. On the other hand, the shoulder appears just when the intermediate is expected to yield a sharp feature so that it is difficult to believe that they are not related. There is no evidence for the shoulder at low temperature (<220 K) where the helix remains folded (the shoulder should be resolvable if it were present).

What conformation(s) give rise to the middle set of cross sections for the Ac-(AGG)$_5$K+H$^+$ peptide? One obvious candidate is the special structure shown in Figure 12. This partially untwisted helical conformation has an average cross section at 300 K of 245 Å^2. The cross section deduced from the drift time distributions at 300 K (237 Å^2) is slightly, but significantly (>2%) smaller. At 400 K the cross section deduced from the measurements and the calculated cross section are both around 239 Å^2. Thus, the special structure seems to account for the middle set of cross sections at the higher temperatures, but perhaps not at the lower temperatures. However, the cross sections derived for middle feature are not as reliable as those determined for well resolved peaks, particularly for temperatures below 330 K where a clear shoulder is not observed. This additional uncertainty may also explain the unusual temperature dependence for the middle feature.

The stability of the unusual hydrogen bonding pattern in the special structure in Figure 11 probably results at least partly from favorable interactions between the helix macrodipole and the dipoles of the backward pointing hydrogen bonds. An obvious question concerning this structure, is whether its unusual hydrogen bonding pattern is a consequence of glycine's conformational freedom. Is this structure still favored for peptides made up of amino acids with side chains? To examine this issue we converted the glycines into alanines, and then ran MD simulations at 300 K. With the all-alanine peptide, the α-helix is around 70 kJ mol^{-1} lower in energy than the structure in Figure 11. In experiments, AcA$_{15}$K+H$^+$ is found to be an α-helix at room temperature.[21,22] Thus glycine's conformational freedom is necessary for the peptide to adopt the special structure.

In the 300 K simulations the lowest-energy Ac(AGG)$_5$K+H$^+$ helix is around 19 kJ mol^{-1} lower in energy than the lowest-energy globule. Since the helix converts into the globule as the temperature is raised the free energy of the helix must be below that of the globule. The globule is expected to be favored entropically,[43] furthermore, it is likely that more extensive MD simulations will find lower energy globules. So there is not a significant quantitative discrepancy between the relative energies from the simulations and the expected values. The special structure in Figure 11 is 9 kJ mol^{-1} more stable than the helix. If the intermediate has a well-defined structure (like that in Figure 11) it will not be favored entropically, and so it should be lower in energy than the helix.

(43) Okamoto, Y.; Hansmann, U. H. E. *J. Phys. Chem.* **1995**, *99*, 11276−11287.

Compared with the relaxation rates measured in the laser-induced temperature jump experiments, around 10^6-10^7 s^{-1} at 300 K, the rate of helix loss in the unsolvated peptides studied here is substantially smaller: 1.4×10^3 s^{-1} (extrapolated to 300 K). However, the value for the Arrhenius activation energy we obtained, 38.2 ± 1.0 kJ mol^{-1}, is quite close to the activation energies found for helix unfolding of alanine-rich peptides in the laser-induced temperature jump experiments (around 33 kJ mol^{-1}).[9,11] The main difference between the solution phase measurements on the alanine-rich peptides and the results reported here is in the preexponential factor. In the laser-induced temperature jump studies values of $10^{12}-10^{13}$ were obtained, compared to a value of $6.5 \pm 3.7 \times 10^9$ s^{-1} found in our studies. The small value for the preexponential factor for helix loss in Ac-$(AGG)_5K+H^+$ indicates a fairly tight transition state. Such a transition state might be expected to result when a predominantly α-helical structure converts into a conformation with a well-defined structure like the one shown in Figure 11.

Perhaps the most notable feature of the results presented here is the observation that α-helical Ac-$(AGG)_5K+H^+$ peptides do not unfold directly to a random globule, but first convert into an intermediate. This long-lived intermediate survives to significantly higher temperatures before converting (on the millisecond time scale of our measurements) into the globule. The intermediate may be a partially untwisted helical conformation like the special structure shown in Figure 11. It is easy to see how such a partially untwisted helix could be an intermediate along the path between an α-helix and a globule. In fact one of the three special structures found in the 400 K simulations resulted from the untwisting of an α-helix in a fixed temperature MD run. The idea that a helix to coil transition occurs by the helix initially untwisting to an intermediate which then converts into a globule, is quite different from the conventional zipper view of helix 6 coil transitions where the helix unravels from its ends and the transition state is unraveling of the final helix turn. It remains to be seen whether the intermediate exists for a variety of different peptides, or just the one studied here.

Acknowledgment. We thank Jiri Kolafa for use of his MACSIMUS molecular modeling programs, and for his helpful advice. We gratefully acknowledge the support of the National Institutes of Health.

JA004196E